Journal of Flow Chemistry (2020) 10:271–282
https://doi.org/10.1007/s41981-019-00051-y

FULL PAPER

High-throughput preparation of uniform tiny droplets in multiple capillaries embedded stepwise microchannels

Yongjin Cui[1] · Yankai Li[1] · Kai Wang[1] · Jian Deng[1] · Guangsheng Luo[1]

Received: 23 September 2019 / Accepted: 3 November 2019 / Published online: 13 February 2020

Abstract

Microfluidic technologies are reliable methods to obtain uniform and tiny droplets, but their application is limited by the capacity of single microchannel and the difficulty in fabrication and operation of large amounts of parallel droplet generators. Here, we reported a microchannel device equipped with multiple capillaries for rupturing the dispersed fluid, which realized droplet generation frequency up to 40 kHz in a single microchannel. The microchannel was operated under jetting flow, which was robust for controlling the droplet size uniformity; therefore, the device did not need highly precise machinery and accurate installation during fabrication. 30–100 μm droplets with CV <5% were successfully prepared in a 20-capillary embedded microchannel device with high throughput, verifying the effectiveness of improving the working ability of micro-channel unit in the scale-up of microfluidic device.

Keywords Droplet generation · High throughput · Microfluidics · Emulsification

Introduction

Uniform droplets in emulsions are ideal templates for preparing uniform spherical materials, which have been widely used in the fields of optical display [1, 2], material structure construction [3], instrument calibration [4, 5] and velocimetry detection [6, 7]. Although highly required in practice, the preparation of uniform and tiny droplets is rather difficult via conventional emulsification methods, such as mechanical agitation and phacoemulsification [8]. Microfluidic approaches overcome the randomness of droplet break-up due to the stability of laminar flow, which have attracted the attention from academic and industry for over 20 years [9–11]. However, this advanced method has not been widely used in industry, due to the low throughput of microchannel [12]. Numbering-up microfluidic droplet generator is thus necessary for preparing sufficient droplets and a lot of reports have shown the concepts of numbering-up microchannels in recent years [13, 14]. Significant progresses have been achieved such as the classical "microchannel emulsification" device from the group of Nakajima et al. [15, 16], based on spontaneously droplet break-up mechanism, and the "large-scale integration chip" proposed by Nisisako and Torii [17], containing hundreds of microchannel junctions. Those studies showed the feasibility of increasing the number of microfluidic droplet generators from a technical point of view, but regrettably, larger scaled numbering-up examples are still less reported. The bottleneck of microfluidic scale-up is mainly from the complex and costly fabrication, which are difficult to be handled, especially for the research groups without automated processing platform. In addition, the fabrication processes based on lithography or chemical etching also limit the material selection of microfluidic equipment. Apart from fabrication, running the microfluidic device with massive number of

Yongjin Cui and Yankai Li contributed equally to this work.

Article Highlights
1. Mass preparation of uniform droplets at 30-100 μm was realized by using low-cost microchannel device.
2. The jetting flow pattern was robust for controlling the droplet size and uniformity.
3. Droplet generation frequency up to 40 kHz was realized for a single microchannel embedded with 10-capillaries.

Electronic supplementary material The online version of this article (https://doi.org/10.1007/s41981-019-00051-y) contains supplementary material, which is available to authorized users.

✉ Kai Wang
kaiwang@tsinghua.edu.cn

✉ Guangsheng Luo
gsluo@tsinghua.edu.cn

[1] The State Key Lab of Chemical Engineering, Department of Chemical Engineering, Tsinghua University, Beijing 100084, China

channels is also challenging because of the difficulty in keeping the robustness of a highly complex piping network. Previous result has shown that uniform droplets cannot be prepared even in fully consistent parallel microchannels without a robust droplet generation process [12]. Therefore, reliable principle and technology for microfluidic scale-up are still waiting to be discovered.

In order to develop low-cost and versatile microfluidic droplet generation methods, we kept on trying to improve the direct quantitative scale-up method of microchannel structures. Our work therefore focused on two issues: one is whether it is possible to use sub-millimeter channel that is easy to fabricate by traditional mechanical method to obtain tiny droplets with diameters less than 100 μm, and the other is how to increase the droplet generation frequency in a microchannel to reduce the number of parallel droplet generators. To answer the first question, we have made some attempts, including improving the microchannel structure with narrowing flow path [18, 19] and coupling gas-liquid phase transition process with the droplet generation process [20, 21]. In these studies, a stepwise microchannel with an embedded capillary was proposed to generate tinny droplets [22, 23]. It can be made from traditional materials by end milling, and it also just employed the commercial capillaries made from metal, glass or quartz. 20–100 μm uniform droplets with diameters 1–2 orders of magnitude smaller than the hydraulic diameter of the microchannel had been successfully prepared in the capillary embedded microchannel [22, 24], with the consumption of relatively high flow rate of shearing fluid. However, this cost was acceptable from the engineering point of view for using a big channel, and most of the shearing fluid was easy to be recycled during the experiment for the stable composition of the surfactant aqueous solution.

Although the capillary embedded stepwise microchannel simplified the fabrication of microfluidic device, the highest droplet generation frequency in it was still less than thousand hertz, which did not reach the level of other multichannel microfluidic device with droplet generation frequencies up to 10 kHz [25–27]. We therefore tried to increase the working capacity of the stepwise microchannel by assembling more capillaries for droplet generation. In this paper, we will show an assemble strategy based on the fluidic dynamic characters of jetting flow in the stepwise microchannel. With careful design of the capillary array and the flow resistance of the dispersed fluid, ten capillaries were successively embedded in one microchannel, which significantly increased the number of generated droplets. The microchannel did not require highly precise machining and accurate installation, and its main parts were all low-costly commercial components. Due to the effective enhancement of droplet generation, the multi-capillary embedded microchannel structure would be a new direction for the improvement of microfluidic scale-up technology.

Results and discussion

Fluid dynamic characteristics of the capillary embedded stepwise microchannel

The basic structure of the capillary embedded stepwise microchannel that made from polymethylmethacrylate (PMMA) plates and a quartz capillary (ZHONGKEKAIDI Co., Ltd., Lanzhou) with outer and inner diameters (d_{c1}) of 740 and 530 μm respectively, is shown in Fig. 1(a). The microchannel had equal width (W_1) and height (H_1) at 750 μm; therefore, the capillary fit well with the microchannel. The capillary head was flush to the edge of the upstream channel as shown in Fig. 1(b), leaving a gap between the tip and the opposite channel wall, whose height (h) was close to 200 μm. On both sides of the stepwise channel, two assistant channels were fabricated to connect a pressure drop sensor (Herdi Central Control, 0–5000 ± 5 Pa) by Teflon tubes (0.9 mm inner diameter), as shown in Fig. 1(a). After fixing the position of the capillary, a sealant (914 Haiyan, China) was used to seal the gap between the PMMA chip and the capillary. This sealant was a high viscous fluid before solidification and we stack it one the side of the PMMA chip. Then, the sealant blocked the gaps 6 h later. By carefully selecting the amount of the sealant, it would not permeate into the stepwise channel.

During the experiment the shearing fluid containing 50 wt% glycerin, 49 wt% water, and 1 wt% sodium dodecyl sulfate (SDS) had a viscosity of 6.92 mPa·s at 25 °C, and *n*-hexane (99%+, Sinopharm) was selected as the dispersed fluid, which was a typical model fluid to study the droplet generation in microchannels [19, 28, 29]. The interfacial tension between the two phases was 4.7 mN/m at 25 °C. (Other details of the fabrication and operation of the microfluidic droplet generator can be found in the Experimental Section.) The stepwise microchannel provided a high shearing velocity at the capillary tip and promoted the break-up of the dispersed fluid [22]. Figure 1(c) exhibits a droplet generation process captured by a microscope with a high-speed CMOS camera (BX51 and i-SPEED TR, at 7000 f/s, Olympus). The average velocity of the shearing fluid reached 0.3 m/s at the capillary tip; thus, tiny droplets that were much smaller than the channel width were continuously prepared. The flow rate ratio of the shearing fluid to the dispersed fluid could be higher than 1000 during the experiment, which was the cost to prepare tiny droplets in this sub-millimeter device. However, the shearing fluid (the aqueous phase) and the dispersed fluid (the oil phase) were immiscible. We therefore stored the outcome fluid in glass bottles. After the droplets were collected from the upper layer of the mixture, the aqueous phase was directly reused in the other experiment. The very little amount of surfactant adsorbed at the oil-water interface almost did not affect the surfactant concentration in the aqueous solution due to the

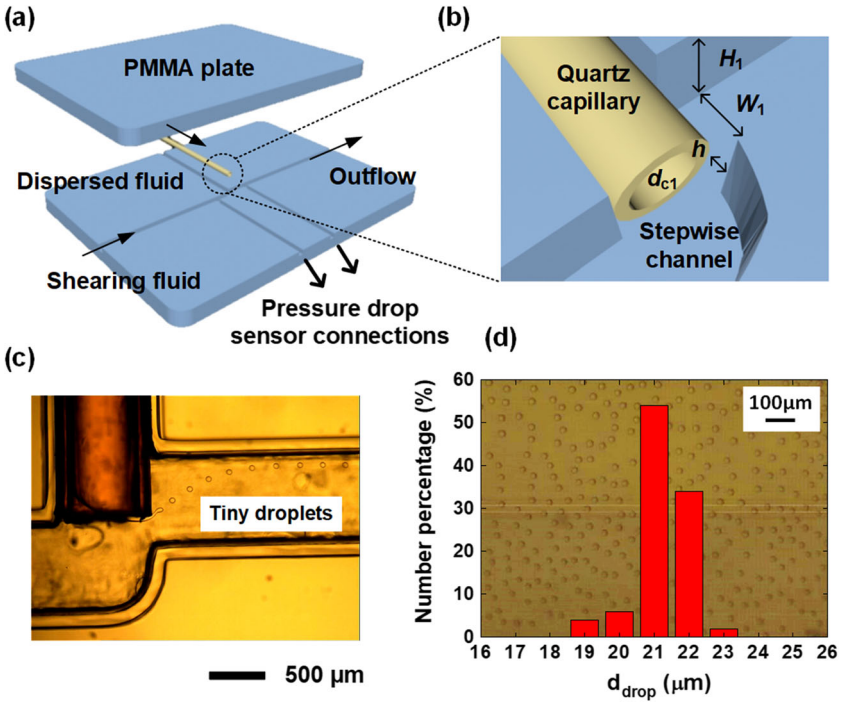

Fig. 1 Schematics and pictures of the capillary embedded stepwise microchannel. **a** Assembly of the microchannel device. The light arrows show the flow directions and the heavy arrows show the connection positions to the pressure drop sensor. **b** Local view of the stepwise microchannel. **c** Microscope picture of the droplet generation at Q_{shear} = 1000 μL/min and Q_{dis} = 10 μL/min. **d** Typical picture of the generated droplets. The CV of droplet diameter was 3.9%. Experiment at Q_{shear} = 1500 μL/min and Q_{dis} = 1 μL/min

large flow rate ratio in the droplet generation; therefore, the shearing effect of the continuous fluid used recycled aqueous phase did not decline. An example of the droplets collected from the stepwise microchannel is shown in Fig. 1(d). The average droplet diameter is 21.6 μm and the diameter distribution quantified by the CV (variable coefficient) defined by Eq. 1 is less than 5%, which is called monodispersed droplets in the microfluidic studies.

$$\mathrm{CV} = \frac{\delta}{d_{\mathrm{av}}} \times 100\% \tag{1}$$

where CV is the ratio of standard deviation (δ) to the average value (d_{av}) of the droplet diameter.

To fully exhibit the fluid dynamic characteristics of the capillary embedded stepwise channel, we carefully studied the droplet size variations, and the results are shown in Fig. 2(a). Different from the T-junction microchannels in general [30, 31], the variation of droplet diameter from the stepwise microchannel has two different regions in respect to the flow patterns of dripping and jetting flow [32, 33]. For the droplets from dripping flow, their diameters mainly relied on the flow rate of the shearing fluid. However, for the jetting ruptured droplets, their diameters varied little with the flow rate increase of the shearing fluid. Only the flow rate of the dispersed phase slightly affected the droplet size, meaning that the droplet size can be fixed in a flow rate region of the continuous phase. According to our previous analysis [22], the droplet diameter was a function of $(Q_{dis}/Q_{shear})^{1/2}$. This droplet size law also means that the requirement for uniform flow rate distribution of the shearing fluid is not necessary in the numbering-up of droplet generators, inspiring us that jetting flow is an ideal flow pattern to realize microfluidic scale-up. In addition, because the flow rate of the dispersed fluid was much lower than the flow rate of the shearing fluid in the capillary embedded stepwise microchannel, the production solution containing tiny droplets had almost the same flow rate as the fresh shearing fluid, which can be used to shear another stream of the dispersed fluid without any significant influence on the second droplet generation. These effects and characters constitute the theoretical foundation of the multi-capillary embedded microchannel we proposed in this article.

Before the scale-up of the microchannel, we investigated two more issues. One was the effect of installation accuracy on the droplet diameter and the other was the pressure drop along the droplet generator, which was important for the feasibility of numbering-up process. Since the stepwise microchannel was fabricated by precisely CNC milling machine, the structure error of the microchannel (<20 μm) could be neglected, and the commercial quartz capillary also had good consistency. Therefore, the structural error of the microchannel mainly came from the assembly of capillaries, which was manually carried out. Trying to control the height of the gap (h) to 150 μm, we randomly obtained h = 108, 165 and 185 μm in 3 tests, respectively. Although some numbers were far from the design value, we can find the droplet sizes were almost the same when the flow rate ratio was fixed, as shown in Fig. 2(b). One reason for this phenomenon was the capillary cannot strictly block the channel for its round cross-section; therefore, the variation of h from 108 to 185 μm did

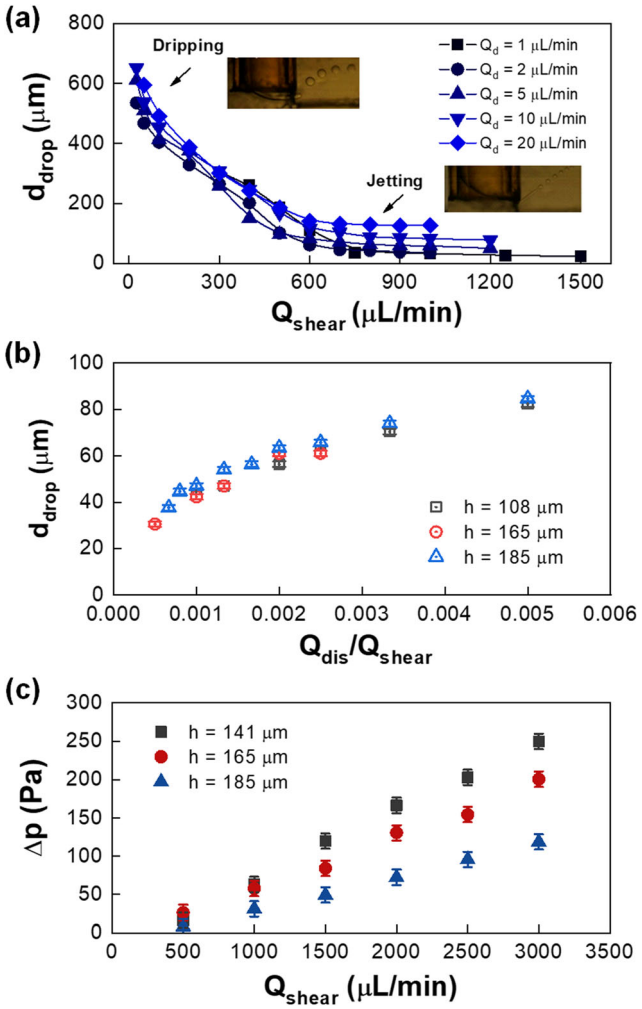

Fig. 2 Droplet generation rules in the capillary embedded stepwise microchannel. **a** Size variation with varied flow rates of two phases. The gap between the capillary tip and the channel wall (h) was 150 μm in height. **b** Effect of gap height on the droplet average diameter at different flow rate ratios. **c** Pressure drops along different droplet generators with heights from 141 to 185 μm, which are basically linear with the flow rates of the shearing fluid. $Q_{dis} = 0$ μL/min in this experiment

not greatly change the area of the cross-section for shearing fluid to pass, which had been demonstrated in our previous work [22]. The other reason was that the shearing velocity had little effect on the droplet diameter under the jetting flow, which exhibited the robustness of this droplet generator. With this good property, we did not need to worry about the effect of the installation accuracy during the scale-up studies. The pressure drop along the droplet generator was given in Fig. 2(c) in which the results showed that the pressure drop along the droplet generator was on the range of hundred Pascal. The pressure drop basically had a linear relationship with the flow rate of the shearing fluid, contributing to >98% of the total flow rate. Different from the droplet size law, the pressure drop along the droplet generator was sensitive to the height of the gap; therefore, the capillary installation accuracy would affect the pressure distribution along the microchannel.

Fundamentals of the multi-capillary embedded stepwise microchannel

After the droplet generation study in the single capillary embedded stepwise micro-channel, we further tried to discover the rules for scaling-up of this droplet generation structure. For the novel number-up method with more than one embedded capillary, the mutual interference between the upstream and downstream droplet generators should be carefully considered. Thus, a dual-capillary embedded channel was developed first, as shown in Fig. 3. The device had two functional layers exhibited by Fig. 3(a) and (b). The upper layer with step structures was used to generate droplets, and the bottom layer with a chamber ($W_2 \times H_2 = 3 \times 1$ mm^2) was used to distribute the dispersed fluid into the side capillaries at the corresponding positions of the capillaries in the upper layer. The capillaries in the up and down layers were connected by Teflon tubes with 0.9 mm inner diameter. The droplet generation layer was source from the microchannel shown in Fig. 1(a), which had improved by the two embedded capillaries. The distance between those capillaries is shown by L in the figure. The capillary inner diameters d_{c1} were both 530 μm. Beside the stepwise microchannel, assistant fluid paths were also made to connect the pressure drop sensor as shown in Fig. 3(a). The inner diameters of capillaries in the fluid distribution layer (d_{c2}) were varied from 530 to 50 μm for turning the resistance of the dispersed fluid. The lengths of all capillaries were 3 cm. The channel fabrication and sealing were the same as the single capillary embedded device.

To study the effect of capillary distance, we firstly equipped the droplet generation layer with independent syringe pumps for the dispersed fluids. (The fluid distribution layer was not used in this experiment.) Typical experimental phenomena were shown in Fig. 4(a). Droplet generation processes with capillary distances from 0.94 to 2.34 mm were tested and we got different droplet uniformities. The dual-capillary embedded stepwise microchannel produced non-uniform droplets at $L = 0.94$ and 1.140 mm; but uniform droplets at $L = 1.54$ and 2.34 mm. These results exhibited that we could not reduce the capillary distance without any limitation. To further understand the principle behind this phenomenon, we measured the flow field in the microchannel with a micro-PIV (microscopic particle image velocimetry, Dantech Dynamics), whose experimental details are shown in the Experimental Section. A result was given by Fig. 5(a), where the velocity strength is shown by the arrow color, and the directions are exhibited by the arrow directions. Figure 5(a) shows that the microchannel gap turns both the velocity strength and direction, and therefore a certain distance is required to lead the velocity field to fully develop to parabolic distribution in the downstream

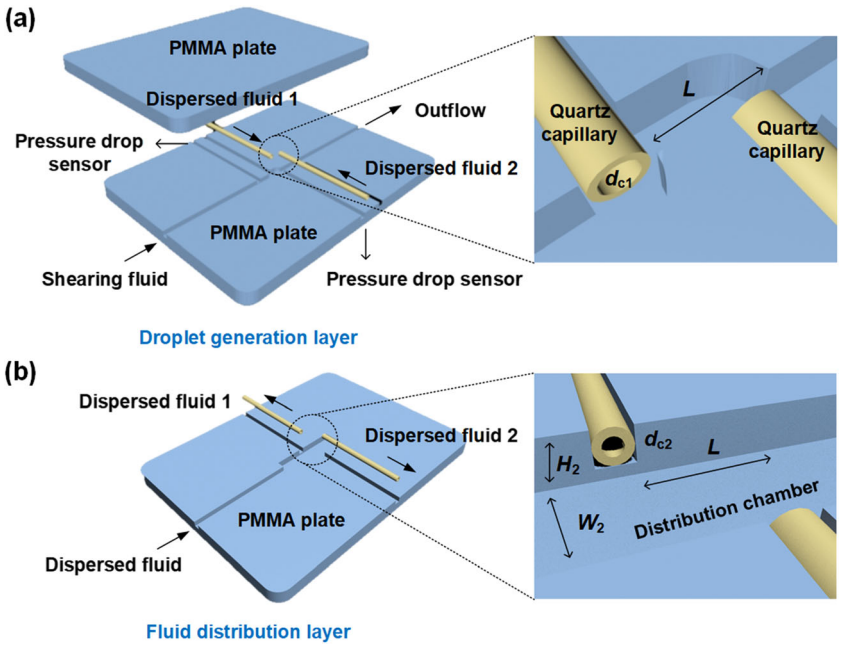

Fig. 3 Schematics of dual-capillary embedded stepwise microchannel. **a** Assembly of the droplet generation layer and local view of the two stepwise microchannel. *L* shows the distance between capillaries. **b** Assembly of the dispersed fluid distribution layer and the local view of the distribution chamber at the bottom of the device

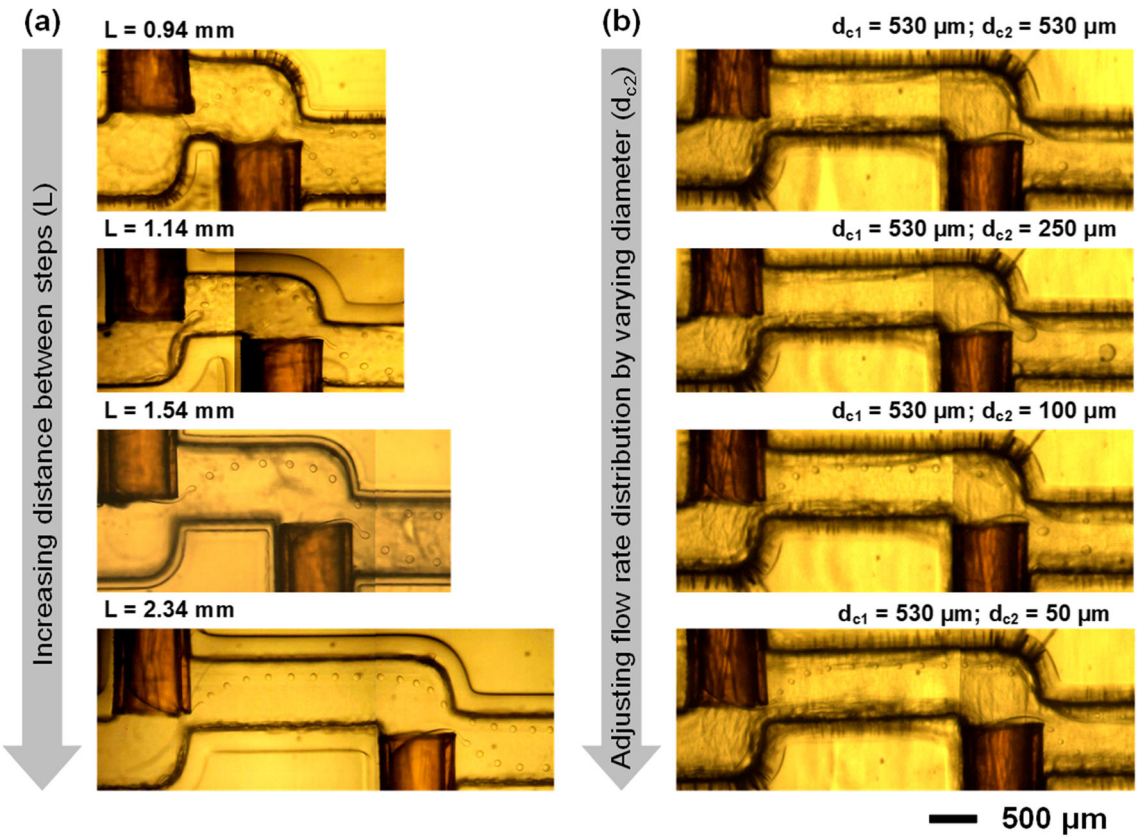

Fig. 4 Pictures of droplet generation experiment with different capillary distances in the droplet generation layer and different capillary diameters in the fluid distribution layer. **a** Effect of capillary distance on the droplet size distribution. Experiment was at $Q_{shear} = 2000$ µL/min and $Q_{dis} = 4$ µL/min for each capillary controlled by independent syringe pumps. **b** Effect of capillary diameters in the fluid distribution layer. The capillary diameters in the droplet generation layer (d_{c1}) was constant at 530 µm, and the capillary diameters in the fluid distribution layer (d_{c2}) varied from 530 to 50 µm. Experiment was at $Q_{shear} = 2000$ µL/min and $p_{dis} = 47$ to 58 kPa. $h = 160 \pm 20$ µm in the microchannels. Image stitching technology was used, due to the view limitation of microscopic field

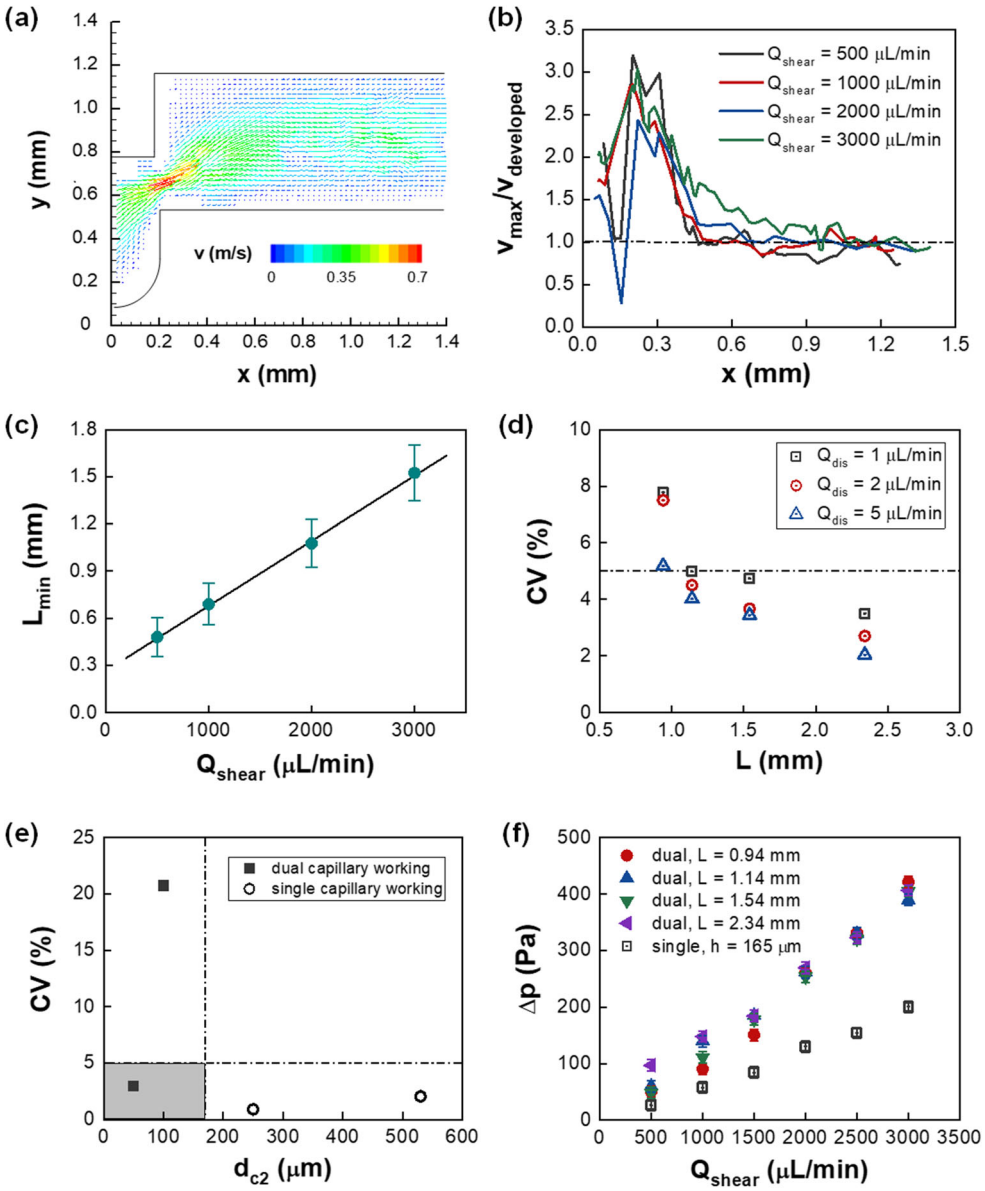

Fig. 5 Droplet generation results in the dual-capillary embedded stepwise microchannel. **a** PIV experimental results, where the arrow color shows the strength of the velocity. The profile of the stepwise microchannel is shown by solid lines. **b** Variations of the maximum velocity along the microchannel with the comparison of fully developed flow velocity at the microchannel center. **c** The minimum distance for developing to the parabolic fluid velocity distribution in the downstream channel of the droplet generator. **d** Variations of droplet size CV with the dispersed fluid and capillary distance. Q_{shear} = 2000 μL/min. **e** Droplet diameter CVs at different capillary diameters in the fluid distribution layer. **f** Pressure drop along the stepwise microchannels with dual- and single capillary

microchannel. Using the data from the micro-PIV experiment, we collected the maximum velocity in certain distances from the capillary, and calculated the ratio of this maximum velocity to the center velocity of the fully developed flow ($v_{max}/v_{developed}$), as shown in Fig. 5(b). The variation of $v_{max}/v_{developed}$ clearly shows that the minimum distance to reach parabolic distribution of fluid velocity (L_{min}, defined the shortest distance at $v_{max}/v_{developed} < 1.05$) is determined by the flow rate of the shearing flulid, and Fig. 5(c) gives an empirically linear relationship between L_{min} and Q_{shear} in experiment. This minimum distance is an important reference to arrange the positions of capillaries. Figure 5(d) shows that at $L > L_{min}$, the CVs of droplet diameter are <5%.

After excluding the influence of flow field development on the droplet generation, we further considered the flow rate distribution of the dispersed phase. Obviously, syringe pumps cannot be unlimited used in the numbering-up process. We thus focused on driving the dispersed fluid with pressure and tested the fluid distribution chamber. Connecting the capillaries of the droplet generation layer and fluid distribution layer and changing the syringe pumps of the dispersed fluids to a pressure-driven controller (OB1, ElveFlow, details are in the Online Resource), we implemented the experiments shown in Fig. 4(b). First, 530 μm inner diameter capillaries were used both in the fluid distribution chamber layer and the droplet generation layer. The experiment showed that the droplets were only observed at the tip of the second capillary and the first one was failed. The pressure to drive the dispersed fluid was 47 kPa in the experiment, much higher than the pressure drop of the stepwise channel shown in Fig. 4(f). Theoretically, the differences of the pressures at the two capillary tips could be neglected comparing to the high driving

pressure; however, the experiment showed inverse result. We further evaluated the flow resistance along the 3 cm long capillaries, which was the narrowest part in the equipment, with Hagen-Poiseuille equation, and the results showed that the pressure drop along the capillary Δp' was only 0.91 Pa at Q_{dis} = 2 μL/min; therefore, the 47 kPa driving pressure should be mainly used to balance the flow resistance in the delivery pipelines. According to the force balance for controlling the droplet generation, the lowest pressure drop between the fluid distribution chamber and the stepwise micro-channel should be larger than the Laplace pressure in the droplet generation capillary, otherwise the additional pressure from the curved liquid-liquid interface will block the pass of the dispersed fluid [34]. Therefore, the pressure in the fluid distribution chamber was not enough to break through the Laplace pressure in the capillary of the first droplet generator, making it failed to generate droplet. In order to rise the pressure in the fluid distribution chamber, we had to increase the resistance of all capillaries. We therefore reduced the inner diameter of the capillaries in the fluid distribution layer from 530 to 50 μm. The experimental pictures in Fig. 4(b) show that both capillaries were working, as d_{c2} reduced to 100 μm, and the counted results in Fig. 5(e) show that only the device with 50 μm capillaries prepared uniformed droplets at a feeding pressure of p_{dis} = 58 kPa. We further evaluated the pressure drop long the capillaries with Hagen-Poiseuille equation, and the results show that the pressure drops were 3.86, 150.8 and 2412 Pa for the 250, 100 and 50 μm capillaries respectively at Q_{dis} = 2 μL/min. According to Fig. 5(f), the pressure drop along one droplet generator was about 120 kPa at Q_{shear} = 2000 μL/min; thus, only the 50 μm capillaries created enough pressure drop to eliminate the influence of pressure distribution along the channel, which was necessary for realizing a symmetric flow rate distribution of the dispersed fluid. Figure 5(f) also shows that the pressure drop between two droplet generators is basically twice of the pressure drop of one droplet generator. In contrast to the gap caused by the embedded capillary, the local hydraulic resistance of the other parts of the microchannel could be neglected, since the pressure drop varied little as we increased the distance between droplet generators.

Design and verification of a 10-capillary embedded stepwise microchannel

After understanding the droplet size and pressure drop variation rules in the dual-capillary embedded stepwise microchannel, we tried to assemble more capillaries to increase the number of generated droplets. Principle of the arrangement of multiple capillaries in single microchannel is shown by Fig. 6(a), where the flow path network is constructed by considering the main flow resistances: capillary resistance in the fluid distribution layer and the resistance of the gap in the stepwise channel. In this network, the pressure drop along the capillaries (Δp_n') should be much larger than the pressure drop along the droplet generation gap (Δp_n) to lead uniform flow rate distribution of the dispersed fluid, as Eq. 2 exhibited.

$$\Delta p_1' = \Delta p_2' = \Delta p_n' >> \Delta p_1 + \Delta p_2 + \cdots + \Delta p_n \quad (2)$$

where n is the number of droplet generators. We therefore decided to use twice length of capillaries (6 cm long and 50 μm inner diameter) in the fluid distribution layer, which could create several thousand Pascal pressure for the fluid to be distributed, and set the gap height to 190 μm, which cost <100 Pa pressure drop along the droplet generator at Q_{shear} < 3000 μL/min referring to the results in Fig. 2(c).

After confirming the parameters of the main components, we designed a 10-capillary embedded stepwise microchannel, as shown in Fig. 6(b). The same as the dual-capillary embedded microchannel, the new device had two layers for droplet generation and fluid distribution, respectively. Local views of the layers are in Fig. 6(c) with arrows showing the flow directions of the dispersed phase. The microchannel steps were alternately placed in the droplet generation layer with 530 μm inner diameter capillaries, and the 50 μm inner diameter capillaries were arranged at the corresponding bottom positions connected to the sides of a 3 × 1 mm^2 cross-section flow rate distribution chamber. The distance between droplet generators L was designed to 2.5 mm, which was about 1.6 times of L_{min} at Q_{shear} = 3000 μL/min, to make sure of the complete development of the flow field in the microchannel. The capillaries in two layers were connected by 0.9 mm inner diameter Teflon tubes. A picture of the whole device is shown in Fig. 6(d), whose fabrication and sealing techniques are the same as above. Delivering the dispersed fluid by pressure-driven controller and the shearing fluid with a syringe pump, we tested the 10-capillary embedded stepwise microchannel, and a typical experiment for the droplet generation process is shown by Fig. 7. The experiment was carried out at Q_{shear} = 3000 μL/min and p_{dis} = 70 kPa with n-hexane as the dispersed fluid and SDS glycerin aqueous solution as the shearing fluid. Pictures show equal sized droplets from every droplet generator and the counted results showed 32 μm average droplet diameter with CV = 3.6%. Other typical results are shown in Fig. 7(b), exhibited uniform droplet from 30 to 100 μm. A video of the droplet generation process is also attached to the electronic Online Resource of the paper.

Parallel scale-up of multi-capillary embedded stepwise microchannels

The prototype of the 10-capillary embedded stepwise microchannel exhibited that consecutive numbering-up of droplet generator in microchannel was also an effective method for the scale-up of microfluidic droplet generators. Finally,

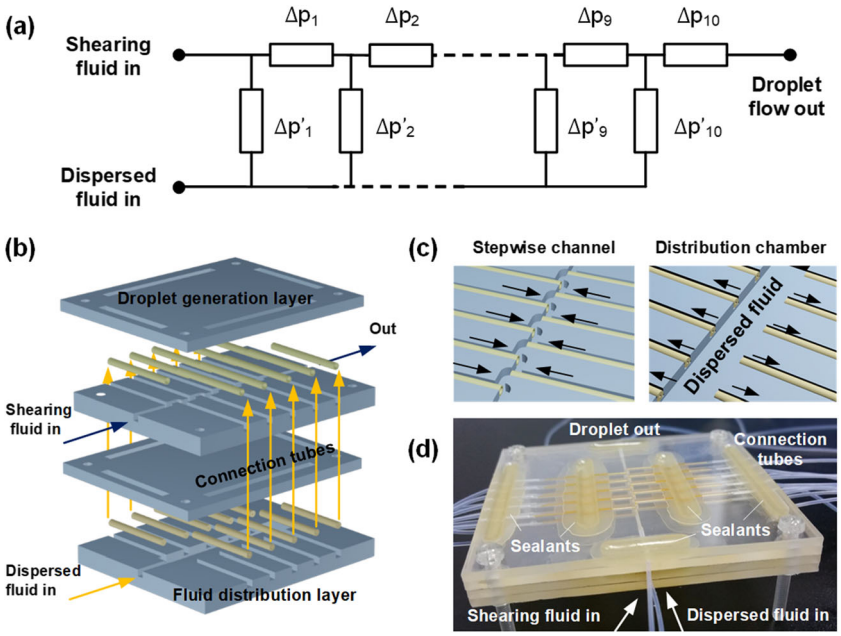

Fig. 6 Principle and schematics of the multi-capillary embedded stepwise microchannel. **a** Pressure drop distribution in the flow path network. Δp_n' is the pressure drop along capillary, and Δp_n is the pressure drop along the droplet generator. **b** Schematic of the microchannel device. The arrows show the flows in connection tubes. **c** Local views of the stepwise microchannel and the fluid distribution chamber. **d** A picture of the microchannel device. The two layers of the chip devices were assembled by PMMA screws and the inner sides of the layers were sealed by the sealants of 914 Haiyan in specially designed grooves

we made a test for the parallel scale-up of the multi-capillary embedded stepwise microchannel, and thus a prototype device with two sets of microchannels was developed, as shown in Fig. 8(a). The parallel microchannels was connected by branched tubes from T-connectors (IDEX Health & Science, inner diameter = 1 mm), whose lengths were strictly controlled to equality. Delivering the shearing fluid by a syringe pump the dispersed fluid by the pressure-driven controller, we obtained the experimental results in Fig. 8(b). Uniform droplets from 30 to 100 μm were also successfully prepared in the microchannel in the flow pattern of jetting flow.

In addition to successful generation of uniform and tiny droplets, we collected the droplet generation frequencies from the recoded videos, which was captured at a frame frequency

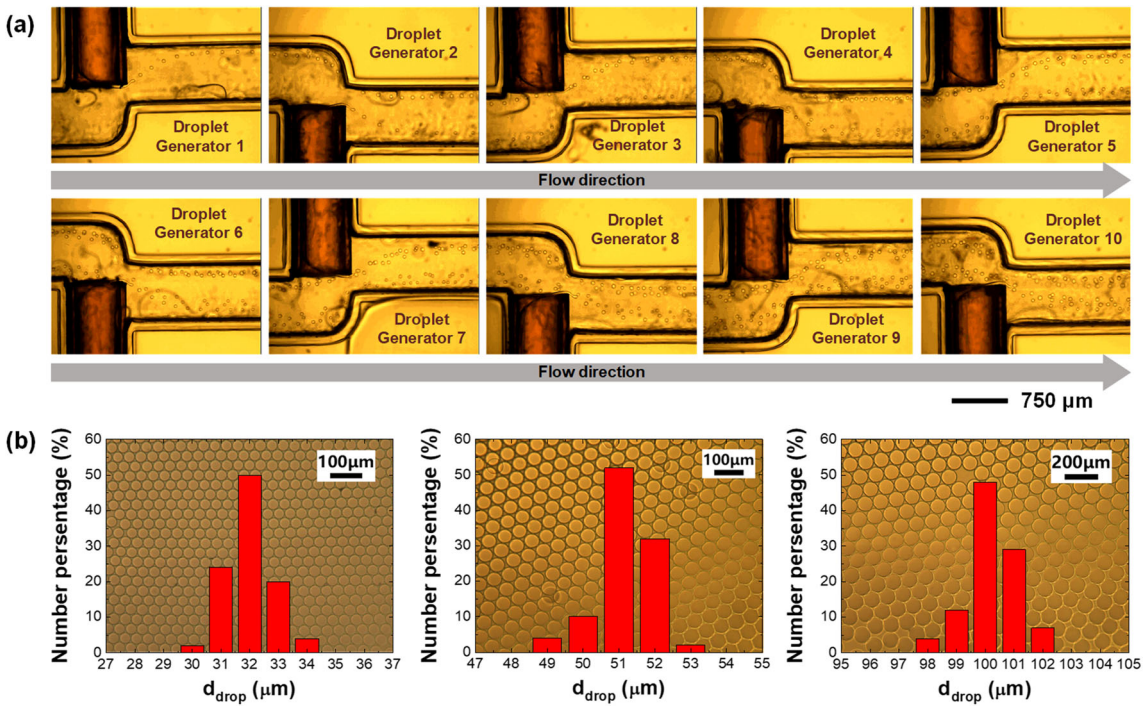

Fig. 7 Pictures of droplet generation processes and some statistical results of the droplet diameters. **a** Droplet generations from different capillaries. **b** Droplet pictures and diameter distributions. More than 100 droplets were counted. Experiment were at Q_{shear} = 3000 μL/min and p_{dis} = 70 kPa for the 32 μm droplets (CV = 3.6%); Q_{shear} = 2500 μL/min and p_{dis} = 73 kPa for the 51 μm droplets (CV = 2.5%); and Q_{shear} = 2000 μL/min and p_{dis} = 101 kPa for the 100 μm droplets (CV = 1.9%)

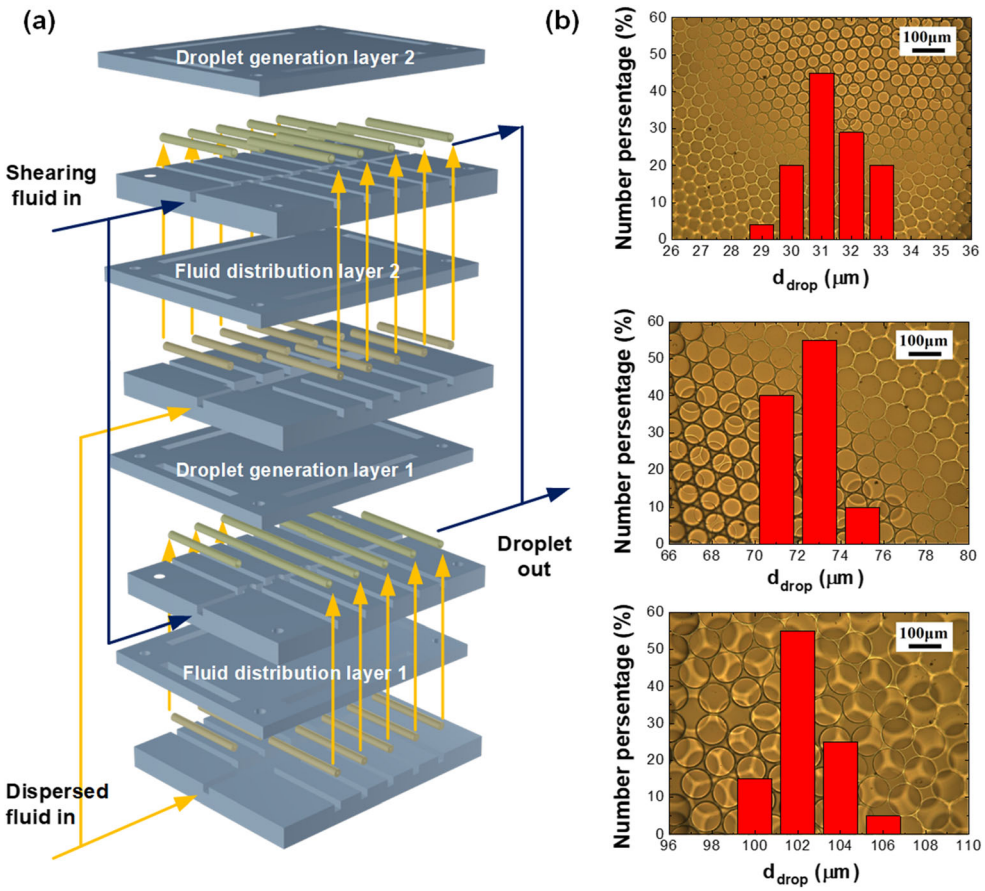

Fig. 8 Schematics of 2 × 10-capillary embedded stepwise microchannels and pictures of uniform droplets. **a** Structure and fluid connections in the microchannel device. **b** Droplet pictures and their size distributions. More than 100 droplets were counted for each condition. Experiments were at Q_{shear} = 6000 μL/min and p_{dis} = 68 kPa for the 32 μm droplets (CV = 4.5%); Q_{shear} = 5000 μL/min and p_{dis} = 81 kPa for the 73 μm droplets (CV = 2.6%); and Q_{shear} = 4000 μL/min and p_{dis} = 100 kPa for the 102 μm droplets (CV = 1.8%)

up to 7000 fps. The results showed that the droplet generation frequency was from 0.5 to 4 kHz in a single droplet generator, and therefore the total droplet generation frequency in the 20-capillary embedded microchannel device had reached to 10–80 kHz, which was rather high. Some experimental results from the literatures were collected in Table 1, which shows that the 20-capillary embedded microchannel device had similar working capacity as those contained hundreds of droplet generators. More importantly, the capillary embedded device successfully prepared <100 μm uniform droplets using sub-millimeter scaled microchannels, which was less reported.

Conclusions

A multi-capillary embedded stepwise microchannel was proposed for realizing high droplet generation frequency in single microchannel. The special design of consecutive droplet generators was based on the robustness of droplet size control of the jetting flow pattern in stepwise microchannel, which was not sensitive to the flow rate variation of the shearing fluid and the installation errors of the capillary position. The key points of arranging the capillary droplet generators were the distance between capillaries, which should be long enough to fully develop the flow field, and the uniform distribution of the flow rates of the dispersed fluid, which was realized by employing high resistance capillaries on both sides of the fluid distribution chamber. Prototype microchannel with ten embedded capillaries were developed, which successfully prepared 30–100 μm droplets with CV < 5%. The highest droplet generation frequency reached 80 kHz in a 20-capillary embedded microchannel device, which was on the same level of the droplet generation devices contained hundreds of parallel microchannels. The multi-capillary embedded stepwise microchannel did not need highly precise fabrication and accurate installation; therefore, it had strong potential to be used in practice.

Experimental

Fabrication of microchannel device

All the stepwise microchannels, the fluid distribution chambers and the channels to place the capillaries were fabricated on polymethyl methacrylate (PMMA) plates with end mills of 0.75 mm diameter. As shown in Figs. 1, 3, 6 and 8, both the height (H_1) and width (W_1) of channels were set to 0.75 mm and the height (H_2) and width (W_2) of the fluid distribution chambers were 1 and 3 mm, respectively. Quartz capillaries

Table 1 Comparison of droplet generation abilities for different microchannels

Numbers of droplet genenerator	Type of droplet genenerator	Substrate & Fabrication	Working system	Channel width (μm)	Droplet Size (μm)	Generation Frequency (kHz)
Parallelization (256×) [35]	Microchannel nozzle	PDMS, by soft lithography	FC-40 oil/SDS aqueous solution	50	40	1.5
Parallelization (512×) [36]	Flow focusing microchannel	PDMS, by soft lithography and laser machining	H_2O/Span80 hexadecane solution	30	75–90	70
Parallelization (550×) [37]	Microchannel nozzle	PDMS, by soft lithography	PEG aqueous soluton/ Fluorinated oil with fluorinated surfactant	50	20–160	15–20
Parallelization (400×) [38]	T-junction microchannel	PMMA, by laser engraving	H_2O/Span80 octane solution	500	800–1200	4
Parallelization (512×) [39]	Flow focusing microchannel	PMMA, by end milling	H_2O/Span20 and Span80 decane solution	250	100–250	10–16
Consecution (10 × 2×) this work	Capillary and microchannel	PMMA, by end milling	Hexane/SDS aqueous solution	750	30–100	10–80

with outer diameter of 0.74 mm were embedded in the side channels with cross-sections of 0.75 × 0.75 mm^2. The height of the gaps between the capillary tips and the channel walls (h) were manually controlled to 100–200 μm. After installation, the microchannel plate was covered by another PMMA plate and sealed at 75 °C and 0.5 MPa for 3 min with a high-pressure thermal sealing machine (A274, Techson, China). The gaps between the capillaries and the side channels were sealed with sealant (914 Haiyan, China). This sealant was a high viscous fluid before solidification and we stick it on the sides of the PMMA chip (single and dual-capillary devices) and or poured it into the grooves (10 and 20-capillary devices) designed to fix the capillaries. The sealant then blocked the gaps after 6 h standing. By carefully selecting the amount of the sealant, it would not permeate into the main channel. Since the PMMA chip was transparent, the positions of the sealants could be confirmed by observation. The microchannels and capillaries were finally connected to the pumps by 0.9 mm inner diameter Teflon tubes (Daxiang Plastics, China).

Materials and droplet generation experimental operation

1 wt% sodium dodecyl sulfate (SDS) and 50 wt% glycerin aqueous solution was used as the shearing fluid, and n-hexane was used as the dispersed fluid in the experiment. The chemicals were from Sinopharm Chemical Reagent Co., Ltd., China. The viscosity of the shearing fluid was 6.92 mPa·s at 25 °C, measured by an Ubbelohde viscometer (Brookfield DV-II + P, USA). The interfacial tension between the two phases was 4.7 mN/m at 25 °C, measured by a pendent drop interface tensiometer (OCAH200, Data Physics Instruments GmbH, Germany). During the experiment, the shearing fluid was fed by a syringe pump (Harvard PHD Ultra, USA) with 200 mL stainless steel syringes, and the dispersed fluid was driven by the same type of syringe pump with 0.5–1 mL glass syringes for the experiments with single and dual-capillary embedded device. For the experiment with more capillaries, the dispersed fluid was pressed by the pressure-driven controller (ElveFlow OB1, France). All the droplet generation processes were recorded by a microscope (BX51, Olympus, Japan) with a high-speed CMOS camera (i-SPEED TR, Olympus, Japan) at 7000 fps. The static pictures of tiny droplets were also captured by the microscope and CMOS camera. The resolution of the high-speed CMOS camera is 1024 × 768, with a scale bar of 0.47 μm/pix. Compared to the measured droplet diameters from experiment (CV = 1.8%~4.5%) in respect to 1.15–1.90 μm in droplet size deviations, the pixel error was much smaller. The pressure drop along the droplet generators was monitored by a pressure drop sensor (HEDI Sensor Instrument, China). The positions of the tunnels for connecting the pressure sensor were shown in Figs. 1(a) and 3(a). The outlets of the tunnels were connected to the pressure drop senor by 0.9 mm inner diameter Teflon tubes.

Microscopic particle image velocimetry (micro-PIV) experiment

The flow field of the shearing fluid shown in Fig. 5(a) was measured by a micro-PIV (Dantec Dynamics, Denmark). 2 μm average diameter fluorescent polystyrene particles (Micro Vec, Inc., China) with 540 nm exciting light were used as the tracing particles. The flow field measuring experiment was implemented without the dispersed fluid, and the shearing fluid was fed by a syringe pump (Harvard PHD Ultra, USA) with 200 mL stainless steel syringe.

Acknowledgements We gratefully acknowledge the supports of the National Natural Science Foundation of China (21991104, 21776150) and National Key R&D Program of China (2017YFB0307102) on this work.

Compliance with ethical standards

Conflict of interest The authors declare that they have no conflict of interest.

References

1. Shang L, Fu F, Cheng Y, Wang H, Liu Y, Zhao Y, Gu Z (2015) Photonic crystal microbubbles as suspension barcodes. J Am Chem Soc 137(49):15533–15539. https://doi.org/10.1021/jacs.5b10612
2. Wang J, Hu Y, Deng R, Xu W, Liu S, Liang R, Nie Z, Zhu J (2012) Construction of multifunctional photonic crystal microcapsules with tunable shell structures by combining microfluidic and controlled photopolymerization. Lab Chip 12(16):2795–2798. https://doi.org/10.1039/c2lc40419b
3. Park JI, Nie Z, Kumachev A, Abdelrahman AI, Binks BP, Stone HA, Kumacheva E (2009) A microfluidic approach to chemically driven assembly of colloidal particles at gas-liquid interfaces. Angew Chem Int Edit 48(29):5300–5304. https://doi.org/10.1002/anie.200805204
4. Sun C, Takegawa N (2018) Calibration of a particle mass spectrometer using polydispersed aerosol particles. Aerosol Sci Technol 53(1):1–7. https://doi.org/10.1080/02786826.2018.1532071
5. Shimada M, Chang H, Fujishige Y, Okuyama K (2001) Calibration of polarization-sensitive and dual-angle laser light scattering methods using standard latex particles. J Colloid Interface Sci 241(1):71–80. https://doi.org/10.1006/jcis.2001.7707
6. Fu T, Ma Y, Funfschilling D, Zhu C, Li HZ (2012) Breakup dynamics of slender bubbles in non-newtonian fluids in microfluidic flow-focusing devices. AICHE J 58(11):3560–3567. https://doi.org/10.1002/aic.13723
7. Walsh PA, Egan VM, Walsh EJ (2009) Novel micro-PIV study enables a greater understanding of nanoparticle suspension flows: nanofluids. Microfluid Nanofluid 8(6):837–842. https://doi.org/10.1007/s10404-009-0553-z
8. Nisisako T (2008) Microstructured devices for preparing controlled multiple emulsions. Chem Eng Tech 31(8):1091–1098. https://doi.org/10.1002/ceat.200800119
9. Zhu P, Wang L (2016) Passive and active droplet generation with microfluidics: a review. Lab Chip 17(1):34–75. https://doi.org/10.1039/c6lc01018k
10. Gu H, Duits MH, Mugele F (2011) Droplets formation and merging in two-phase flow microfluidics. Int J Mol Sci 12(4):2572–2597. https://doi.org/10.3390/ijms12042572
11. Christopher GF, Anna SL (2007) Microfluidic methods for generating continuous droplet streams. J Phys D Appl Phys 40(19):R319–R336. https://doi.org/10.1088/0022-3727/40/19/r01
12. Li W, Young EWK, Seo M, Nie Z, Garstecki P, Simmons CA, Kumacheva E (2008) Simultaneous generation of droplets with different dimensions in parallel integrated microfluidic droplet generators. Soft Matter 4(2):258–262. https://doi.org/10.1039/b712917c
13. Shen Q, Zhang C, Tahir MF, Jiang S, Zhu C, Ma Y, Fu T (2018) Numbering-up strategies of micro-chemical process: uniformity of distribution of multiphase flow in parallel microchannels. Chem Eng Process 132:148–159. https://doi.org/10.1016/j.cep.2018.09.002
14. Yap SK, Wong WK, Ng NXY, Khan SA (2017) Three-phase microfluidic reactor networks – design, modeling and application to scaled-out nanoparticle-catalyzed hydrogenations with online catalyst recovery and recycle. Chem Eng Sci 169:117–127. https://doi.org/10.1016/j.ces.2016.12.005
15. Sugiura S, Nakajima M, Kumazawa N, Iwamoto S, Seki M (2002) Characterization of spontaneous transformation-based droplet formation during microchannel emulsification. J Phys Chem B 106(36):9405–9409. https://doi.org/10.1021/jp0259871
16. Sugiura S, Nakajima M, Seki M (2002) Preparation of monodispersed polymeric microspheres over 50 μm employing microchannel emulsification. Ind Eng Chem Res 41(16):4043–4047. https://doi.org/10.1021/ie0201415
17. Nisisako T, Torii T (2008) Microfluidic large-scale integration on a chip for mass production of monodisperse droplets and particles. Lab Chip 8(2):287–293. https://doi.org/10.1039/b713141k
18. Dong P-F, Xu J-H, Zhao H, Luo G-S (2013) Preparation of 10μm scale monodispersed particles by jetting flow in coaxial microfluidic devices. Chem Eng J 214:106–111. https://doi.org/10.1016/j.cej.2012.10.081
19. Wang K, Lu YC, Xu JH, Tan J, Luo GS (2011) Generation of micromonodispersed droplets and bubbles in the capillary embedded T-junction microfluidic devices. AICHE J 57(2):299–306. https://doi.org/10.1002/aic.12263
20. Wang K, Xie L, Lu Y, Luo G (2013) Generation of monodispersed microdroplets by temperature controlled bubble condensation processes. Lab Chip 13(1):73–76. https://doi.org/10.1039/c2lc40159b
21. Yang L, Wang K, Mak S, Li Y, Luo G (2013) A novel microfluidic technology for the preparation of gas-in-oil-in-water emulsions. Lab Chip 13(17):3355–3359. https://doi.org/10.1039/c3lc50652e
22. Li YK, Liu GT, Xu JH, Wang K, Luo GS (2015) A microdevice for producing monodispersed droplets under a jetting flow. RSC Adv 5(35):27356–27364. https://doi.org/10.1039/c5ra02397a
23. Li YK, Wang K, Xu JH, Luo GS (2016) A capillary-assembled micro-device for monodispersed small bubble and droplet generation. Chem Eng J 293:182–188. https://doi.org/10.1016/j.cej.2016.02.074
24. Li YK, Wang K, Luo GS (2017) Microdroplet generation with dilute surfactant concentration in a modified T-junction device. Ind Eng Chem Res 56(42):12131–12138. https://doi.org/10.1021/acs.iecr.7b02588
25. Nisisako T, Ando T, Hatsuzawa T (2012) High-volume production of single and compound emulsions in a microfluidic parallelization arrangement coupled with coaxial annular world-to-chip interfaces. Lab Chip 12(18):3426–3435. https://doi.org/10.1039/c2lc40245a
26. Kim M, Pan M, Gai Y, Pang S, Han C, Yang C, Tang SK (2015) Optofluidic ultrahigh-throughput detection of fluorescent drops. Lab Chip 15(6):1417–1423. https://doi.org/10.1039/c4lc01465k
27. Lim J, Caen O, Vrignon J, Konrad M, Taly V, Baret JC (2015) Parallelized ultra-high throughput microfluidic emulsifier for multiplex kinetic assays. Biomicrofluidics 9(3):034101. https://doi.org/10.1063/1.4919415
28. Wang K, Lu YC, Xu JH, Luo GS (2009) Determination of dynamic interfacial tension and its effect on droplet formation in the T-shaped microdispersion process. Langmuir 25(4):2153–2158. https://doi.org/10.1021/la803049s
29. Wang K, Zhang L, Zhang W, Luo G (2016) Mass-transfer-controlled dynamic interfacial tension in microfluidic emulsification processes. Langmuir 32(13):3174–3185. https://doi.org/10.1021/acs.langmuir.6b00271
30. Ushikubo FY, Birribilli FS, Oliveira DRB, Cunha RL (2014) Y- and T-junction microfluidic devices: effect of fluids and interface properties and operating conditions. Microfluid Nanofluid 17(4):711–720. https://doi.org/10.1007/s10404-014-1348-4
31. Wehking JD, Gabany M, Chew L, Kumar R (2013) Effects of viscosity, interfacial tension, and flow geometry on droplet formation in a microfluidic T-junction. Microfluid Nanofluid 16(3):441–453. https://doi.org/10.1007/s10404-013-1239-0
32. Utada AS, Fernandez-Nieves A, Gordillo JM, Weitz DA (2008) Absolute instability of a liquid jet in a coflowing stream. Phys

Rev Lett 100(1):014502. https://doi.org/10.1103/PhysRevLett.100.014502
33. Utada AS, Fernandez-Nieves A, Stone HA, Weitz DA (2007) Dripping to jetting transitions in coflowing liquid streams. Phys Rev Lett 99(9):094502. https://doi.org/10.1103/PhysRevLett.99.094502
34. Li S, Xu J, Wang Y, Luo G (2009) A new interfacial tension measurement method through a pore array micro-structured device. J Colloid Interface Sci 331(1):127–131. https://doi.org/10.1016/j.jcis.2008.11.017
35. Dangla R, Kayi SC, Baroud CN (2013) Droplet microfluidics driven by gradients of confinement. Proc Natl Acad Sci 110(3):853–858. https://doi.org/10.1073/pnas.1209186110
36. Muluneh M, Issadore D (2013) Hybrid soft-lithography/laser machined microchips for the parallel generation of droplets. Lab Chip 13(24):4750–4754. https://doi.org/10.1039/c3lc50979f
37. Amstad E, Chemama M, Eggersdorfer M, Arriaga LR, Brenner MP, Weitz DA (2016) Robust scalable high throughput production of monodisperse drops. Lab Chip 16(21):4163–4172. https://doi.org/10.1039/c6lc01075j
38. Han T, Zhang L, Xu H, Xuan J (2017) Factory-on-chip: modularised microfluidic reactors for continuous mass production of functional materials. Chem Eng J 326:765–773. https://doi.org/10.1016/j.cej.2017.06.028
39. Conchouso D, Castro D, Khan SA, Foulds IG (2014) Three-dimensional parallelization of microfluidic droplet generators for a litre per hour volume production of single emulsions. Lab Chip 14(16):3011–3020. https://doi.org/10.1039/c4lc00379a

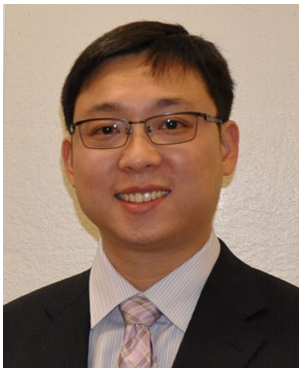

Dr. Kai Wang obtained his Ph. D. degree in 2010 from the Department of Chemical Engineering Tsinghua University, Beijing, China. During 2015 to 2016, he worked as a visiting scholar in the Department of Chemical Engineering, Massachusetts Institute of Technology. He is now working as an associate professor in the State Key Laboratory of Chemical Engineering, Department of Chemical Engineering Tsinghua University. His research interests concern flow chemistry principle and technology, especially for the continuous syntheses of fine chemicals and polymer materials. He has published 115 research papers and filled 35 Chinese patents.